nature astronomy

LETTERS

DOI: 10.1038/s41550-017-0271-5

Disruption of Saturn's quasi-periodic equatorial oscillation by the great northern storm

Leigh N. Fletcher[1*], Sandrine Guerlet[2], Glenn S. Orton[3], Richard G. Cosentino[4], Thierry Fouchet[5], Patrick G. J. Irwin[6], Liming Li[7], F. Michael Flasar[4], Nicolas Gorius[4] and Raúl Morales-Juberías[8]

The equatorial middle atmospheres of the Earth[1], Jupiter[2] and Saturn[3,4] all exhibit a remarkably similar phenomenon—a vertical, cyclic pattern of alternating temperatures and zonal (east–west) wind regimes that propagate slowly downwards with a well-defined multi-year period. Earth's quasi-biennial oscillation (QBO) (observed in the lower stratospheric winds with an average period of 28 months) is one of the most regular, repeatable cycles exhibited by our climate system[1,5,6], and yet recent work has shown that this regularity can be disrupted by events occurring far away from the equatorial region, an example of a phenomenon known as atmospheric teleconnection[7,8]. Here, we reveal that Saturn's equatorial quasi-periodic oscillation (QPO) (with an ~15-year period[3,9]) can also be dramatically perturbed. An intense springtime storm erupted at Saturn's northern mid-latitudes in December 2010[10–12], spawning a gigantic hot vortex in the stratosphere at 40° N that persisted for three years[13]. Far from the storm, the Cassini temperature measurements showed a dramatic ~10 K cooling in the 0.5–5 mbar range across the entire equatorial region, disrupting the regular QPO pattern and significantly altering the middle-atmospheric wind structure, suggesting an injection of westward momentum into the equatorial wind system from waves generated by the northern storm. Hence, as on Earth, meteorological activity at mid-latitudes can have a profound effect on the regular atmospheric cycles in Saturn's tropics, demonstrating that waves can provide horizontal teleconnections between the phenomena shaping the middle atmospheres of giant planets.

Equatorial oscillations in the stratospheres of Earth, Jupiter and Saturn manifest vertical patterns of alternating zonal (east–west) axisymmetric wind regimes (zonal jets) and associated temperature anomalies. For the gas giant planets, where direct stratospheric wind measurements are unavailable, the oscillations are inferred from thermal-infrared observations of the 3D temperature structure, which revealed both Jupiter's 4–5-year period quasi-quadrennial oscillation (QQO[2]) and Saturn's 14.7 ± 0.9-year QPO[3,4]. By analogy to Earth's tropics, the origin and evolution of these middle-atmosphere cycles may be linked to the spectrum of upwardly propagating waves launched by tropospheric convection[4,14]. These waves, with both eastward and westward phase velocities, are damped and preferentially deposit their momentum in regions where the mean zonal flow velocity is near the phase velocity of the wave[15–17]. The wave-induced acceleration causes the pattern of zonal winds to descend downwards over time to ultimately dissipate near the tropopause[18]. Disrupting these regular cycles therefore requires some mechanism to interrupt or modify the wave-induced momentum transport responsible for the stratospheric pattern.

Previous analyses of Saturn's QPO and associated stratospheric jets[9,18–21] lacked good temporal sampling, but suggested that its semi-annual period might display interannual variability. Counter to expectations, a comparison of stratospheric thermal structures between Voyager and Cassini observations at the same point in Saturn's seasonal cycle (two QPO cycles apart in 1980 and 2010) showed significant differences in the equatorial temperature contrasts at 1 mbar between the two epochs[22]. To explore the evolution of this oscillation beyond mere snapshots, we utilized the unprecedented 2004–2017 time series provided by the Cassini Composite Infrared Spectrometer (CIRS)[23], zonally averaging nadir $15\,cm^{-1}$ -resolution spectra spanning $600–1{,}400\,cm^{-1}$ (7.1–16.6 μm), to generate a monthly database between ±30° latitude (see Methods). Each spectrum was inverted to estimate zonally averaged stratospheric temperatures (0.5–5 mbar) and hydrocarbon distributions from methane, ethane and acetylene emission features. Limb-viewing observations with improved vertical resolution[21] were used as anchor points for the time series to confirm consistency with previous studies (see Methods). Interpolation of the time series in Fig. 1 produced animations (Supplementary Videos 1–4) of temperatures, temperature anomalies and zonal winds (see Methods and the Supplementary Information), snapshots of which can be seen in Fig. 2.

Supplementary Videos 1–3 and Fig. 3 show the regular downward propagation of the QPO temperature anomalies before 2011, both at the equator (averaged over ±5°) and in the extra-tropical regions (±16°) associated with secondary circulation patterns, as on Earth[17]. Seasonal temperature changes due to Saturn's 27° orbital obliquity are evident in comparing 2006 (pre-equinox) to 2015 (post-equinox) (Fig. 2) data at latitudes >10° (ref. [20]), but the equatorial temperature field is dominated by the QPO. We estimate that the thermal anomalies descend at a rate of $17 \pm 1\,km\,yr^{-1}$ ($0.5 \pm 0.1\,mm\,s^{-1}$) or ~0.3 scale heights per year at 1 mbar, consistent with previous estimates[9,18]. These warm and cool anomalies are separated by approximately a decade of pressure (2–3 pressure scale heights), and the descent speed remains consistent with a semi-annual cycle. The descent is not likely to be rigid, with some distortion of the shape of the QPO as it descends, but we find no measurable distinction between the descent rates of warm and cool

[1]Department of Physics and Astronomy, University of Leicester, University Road, Leicester LE1 7RH, UK. [2]Laboratoire de Meteorologie Dynamique /IPSL, Sorbonne Universités, UPMC Univ Paris 06, CNRS, Paris, France. [3]Jet Propulsion Laboratory, California Institute of Technology, 4800 Oak Grove Drive, Pasadena, CA 91109, USA. [4]NASA Goddard Spaceflight Center, Maryland, MD 20771, USA. [5]LESIA, Observatoire de Paris, PSL Research University, CNRS, Sorbonne Universités, UPMC Univ. Paris 06, Univ. Paris Diderot, Sorbonne Paris Cité, 5 place Jules Janssen, 92195 Meudon, France. [6]Atmospheric, Oceanic and Planetary Physics, University of Oxford, Parks Road, Oxford OX1 3PU, UK. [7]Department of Physics, University of Houston, Houston, TX 77004, USA. [8]New Mexico Institute of Mining and Technology, Socorro, NM 87801, USA. *e-mail: leigh.fletcher@leicester.ac.uk

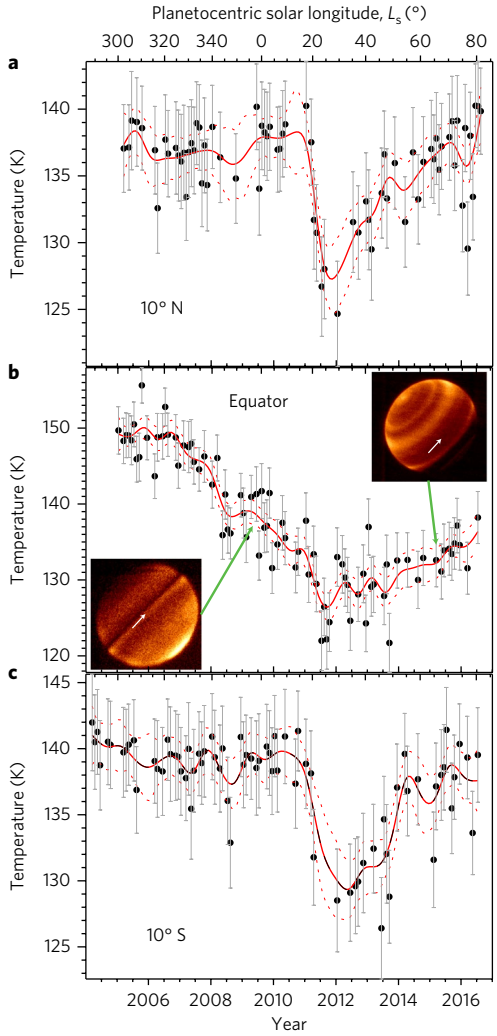

Fig. 1 | Saturn's stratospheric temperatures at 1 mbar determined by Cassini/CIRS. a–c, Tens of thousands of individual mid-infrared spectra were inverted to measure stratospheric temperatures (circles with retrieval uncertainties). Tensioned splines (solid lines with dotted uncertainties) are used to smoothly interpolate the time series. The dramatic cooling associated with the northern storm activity is evident both sides of the equator in **a** and **c** (the storm first erupted on 5 December 2010), with a return to 'pre-storm' temperatures in 2014. Inset images in **b** reveal 7.9-μm methane emission from the VISIR instrument on VLT on 20 April 2009 and 21 May 2015. The white arrows show the equator. These confirm the disappearance of the bright equatorial band as the QPO switched phase (see Methods and Supplementary Information).

anomalies, unlike on Earth where eastward shear zones descend more rapidly than westward shear zones[1].

Cassini arrived at Saturn during northern winter, when the 1-mbar equatorial temperatures were at their peak[20] (Fig. 1b), associated with a strong eastward QPO phase[19] and a bright band at Saturn's equator at 7.8 μm (ref. [3]). The eastward shear zone filters waves of the same velocity, absorbing waves with eastward momentum while allowing waves with westward momentum to propagate into the high stratosphere to cause the onset of a westward phase. The equator cooled ~20 K at 1 mbar as this newer shear zone moved downwards, being coolest in 2012–2014 before starting to recover with the onset of a new eastward phase by 2016. The opposite is seen at 5 mbar, where temperatures increased until 2010 but fell from 2010 to 2017 (Supplementary Information). The removal of the warm equatorial band was evident in ground-based ESO VLT/VISIR and Subaru/COMICS imaging observations at 7.9 and 12.3 μm taken between 2005 and 2016 (Fig. 1b and Supplementary Information), consistent with the switch to the westward QPO phase near 1 mbar (see Methods). However, closer inspection of the 1-mbar temperatures at ±10° latitude in Fig. 1a,c showed that they had been stable over time until a dramatic 10–12 K cooling event in 2011, which persisted until at least 2014. The 'normal' QPO evolution resumed after 2014, but the sudden 2011–2014 perturbation, symmetric about Saturn's equator (Fig. 2) and restricted to pressures, $p < 5$ mbar, was counter to any expectations for the smoothly oscillating QPO.

In December 2010, a planet-encircling storm had erupted in Saturn's northern mid-latitudes (40° N), with powerful convective plumes lofting ices and gaseous species into the upper troposphere[10–12]. The effects on Saturn's stratosphere provided indirect evidence of vertically propagating waves transporting energy and momentum into the middle atmosphere[10,13]. Although the tropospheric storm system abated after 6–8 months, the stratospheric after-effects were evident for more than 3 yrs, with the formation of an enormous, westward-moving hot vortex (the 'beacon'[13]), with temperatures elevated ~80 K above the quiescent stratosphere at 2 mbar. Both the tropospheric storm, and the stratospheric vortex that it spawned, are likely to have generated substantial wave activity, but their impact on tropical temperatures on both sides of Saturn's equator was unexpected.

Stratospheric winds can be estimated by assuming geostrophic balance and using the latitudinal temperature gradients to integrate zonal winds along cylinders parallel to Saturn's rotation axis. This modified thermal wind equation (rather than integrating in altitude) is required because of the proximity to the equator, where the Coriolis parameter vanishes (see Methods). Figures 2 and 3 show stratospheric winds relative to the 5-mbar level, and indicate that the strongly eastward flow observed at the start of Cassini's observing record[19] moved downward from 2004 to 2010. Immediately before the storm onset, a westward phase (relative to the 5-mbar level) was forming at $p < 0.5$ mbar as part of the regular QPO cycle. The 2011 storm eruption initially decelerated the eastward flow throughout the ±10° range near 1–3 mbar, most probably due to an injection of westward momentum, removing the strong eastward windshear near 5 mbar (Fig. 3c). By 2012, when the cooling at ±10° was at its maximum, the windshear had shifted so that weak eastward winds were distributed over the full 0.5–5.0 mbar range, obliterating all signs of the QPO pattern and the weak westward phase that had developed in 2010. However, by 2013, the westward windshear was fully established near 1 mbar (Fig. 3c), such that the westward phase (and the cool equatorial temperatures) prevailed at 1 mbar throughout 2014–2016. This suggests that, despite the 3-yr QPO disruption and the abrupt cooling of the ±10° region, the equatorial oscillation was able to re-establish its standard phase progression. The result was that the strong prograde jet observed at the start of the Cassini mission[19] had been considerably weakened as the QPO switched to the opposite phase. Note that, given that the magnitudes of stratospheric winds are subject to large uncertainties (see Methods), we cannot determine whether the stratospheric winds have switched to retrograde flow during this phase, as they do on Earth, so all winds are given relative to the 5-mbar level. Finally, in 2016, a new region of eastward windshear and warmer temperatures can be seen for $p < 1$ mbar in Fig. 3b,c, signalling the onset of the slow switch back to the eastward phase that was seen at the start of Cassini's observations.

An equatorial injection of westward momentum from the northern mid-latitudes is in agreement with both the westward motion of the stratospheric vortex, the anticyclonic nature of the rising storm plumes[24], and with the hypothesis that the beacon formed through interactions of Rossby and gravity waves forced by tropospheric convection (that is, a source of westward momentum) with the

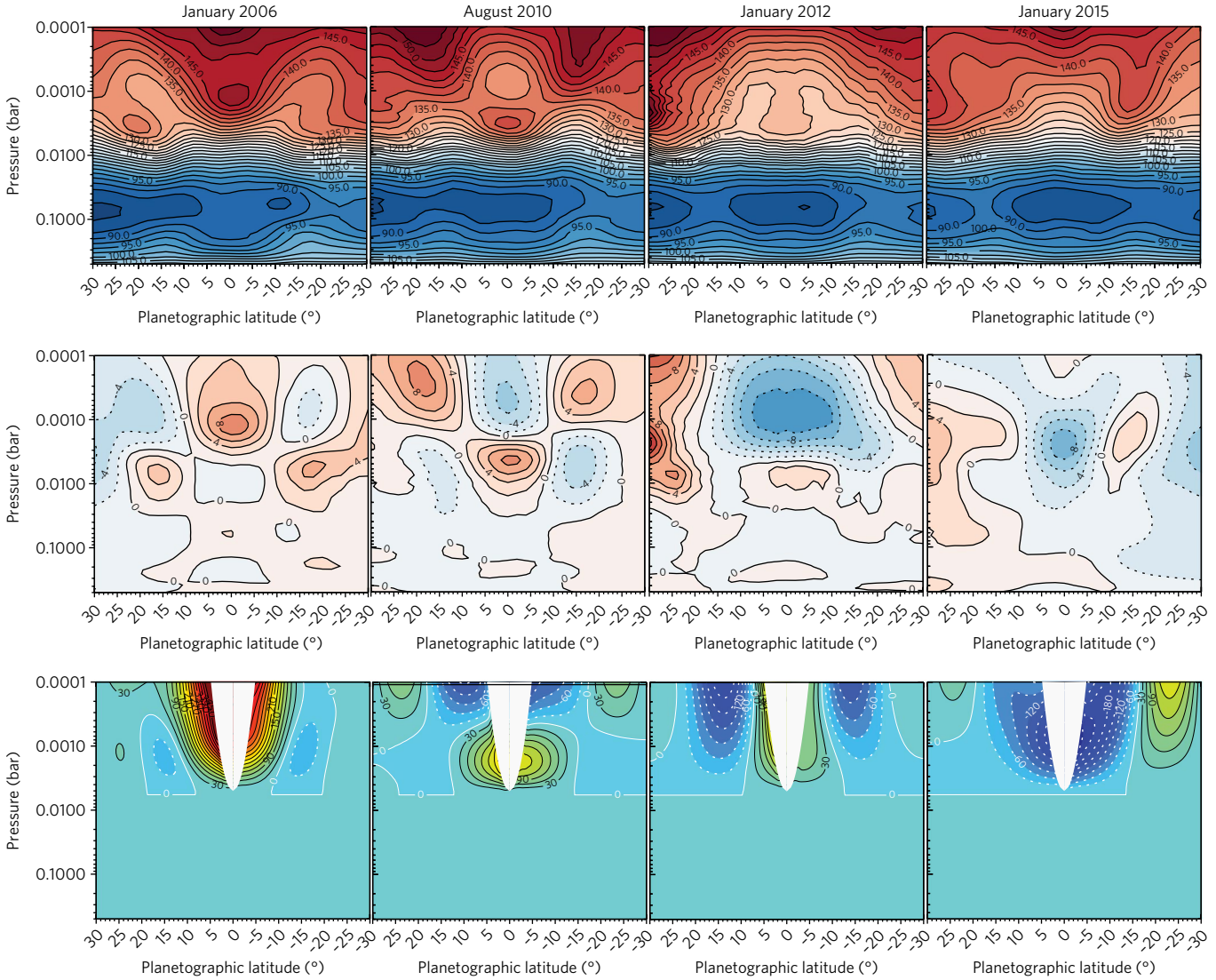

Fig. 2 | Snapshots of Saturn's equatorial temperatures and winds during the 13-yr time series in Fig. 1. The equatorial temperatures are shown in the top and middle rows and winds in the bottom row. The temperature anomaly in the middle row was formed by subtracting a time-averaged temperature profile for each latitude from the data in the top row (excluding 2011–2013). Extra-tropical signatures of the QPO (in antiphase with the equatorial QPO structure) can clearly be seen at ±15–20° in both hemispheres. Zonal winds (bottom row) were calculated from the modified thermal windshear equation, integrating along cylinders parallel to Saturn's rotation axis[9,19,33] from a level of no-motion at 5 mbar, and therefore should be considered as a perturbation on top of the middle-atmospheric winds that are likely to remain eastward at these altitudes (see Methods). Our results do not imply retrograde stratospheric flow. The white parabola indicates regions where the thermal wind calculation is unconstrained[9]. Temperature uncertainties are 2–4 K, but zonal-wind uncertainties are large given the low vertical resolution (see Methods). Temperatures and winds are shown during Cassini's prime mission (2006), before the storm onset (2010), at the maximum equatorial cooling (January 2012), and once the QPO had returned to the expected westward phase (with a cool band at the equator at 1 mbar) in 2015. Supplementary Videos 1–4 provide full animations of the data shown in these figures.

background stratospheric flow[13]. Saturn's middle-atmospheric flow is strongly eastward throughout the low latitudes due to the broad equatorial super-rotating jet[25] and the small vertical windshears away from the equator[10,26], implying an absence of critical surfaces to absorb stationary or westward-moving Rossby waves (that is, those waves moving west with respect to the mean eastward equatorial flow). This means that any waves radiated from the northern storm in three dimensions were not latitudinally confined and could propagate to the equator where they encountered the eastward shear zone of the QPO pattern (Fig. 3c). The perturbation to the QPO pattern was remarkably symmetric about the equator (Fig. 2), with implications as far south as 20° S—a far wider range of influence for the storm than previously thought. Given that Saturn's equatorial jet is also symmetric, this supports the concept of a wave–mean flow interaction, with momentum flux deposition maximized in critical regions near ±10° latitude that depend on the velocity of the background flow. Furthermore, Rossby wave activity is often restricted to low pressures by the static stability[27], favouring the stratospheric vortex as the source of wave-induced westward momentum, rather than the storm itself.

Earth's QBO impacts extra-tropical latitudes via teleconnections, providing a link between weather changes in regions that are geographically separated[28]. Indeed, Earth's QBO was severely disrupted in 2015–2016 by an influx of westward momentum by waves emanating from extra-tropical sources in the northern winter hemisphere, forming a new westward layer within the eastward phase[7,8]. This adjustment was unprecedented in the 66-yr QBO record. The observation of Saturn's QPO disruption during the storm epoch

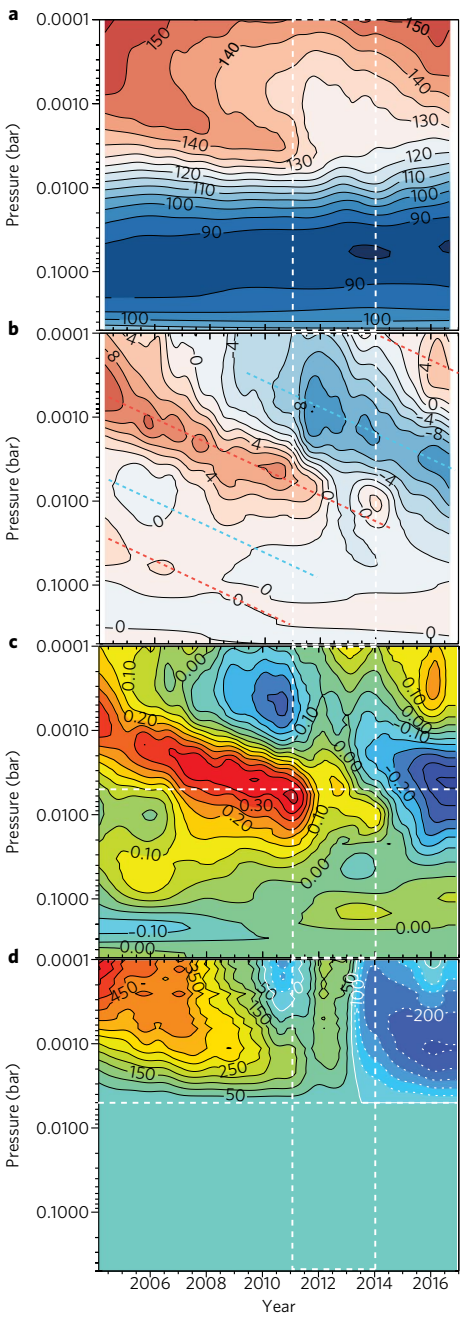

Fig. 3 | Hovmöller diagrams showing the downward propagation of the QPO thermal and wind patterns and the 2011–2014 disruption. **a**–**d**, Equatorial temperatures (**a**; in K); temperature anomalies (**b**; in K); thermal windshear along cylinders parallel to Saturn's rotation axis (in m s^{-1} km^{-1}) estimated from the modified TWE (**c**; see Methods); and zonal winds (**d**; in m s^{-1}) in the $p < 5$ mbar region estimated by integrating the TWE upwards from $u = 0$ m s^{-1} at 5 mbar (that is, only in the altitude region to which nadir data are sensitive, signified by the horizontal white dashed lines in **c** and **d**. The vertical dashed lines at 2011 and 2014 indicate the lifetime of the stratospheric vortex near 40° N (ref. [13]). All values were averaged over ±5° of the equator, although we caution that nadir inversions (1) lack information about the latitudinal temperature gradient in the 5–80 mbar range; and (2) lack vertical temperature resolution that causes significant uncertainty on the magnitude of thermal winds (see Methods). Westward winds (relative to the 5-mbar level) are shown by dashed contours in **d**. Diagonal dotted lines in **b** show the descent of the warm (red lines) and cool (blue lines) QPO thermal anomalies.

suggests that it possesses similar teleconnections between tropical oscillations and mid-latitude weather, despite a separation of ~40,000 km. The perturbations observed in 2011–2014 could have been a unique consequence of the storm's timing, as we would expect the extent of the perturbation to be sensitive to the precise QPO phase, and it will be important to track the QPO behaviour during the next storm outbreak on Saturn. Furthermore, even if the 1990 equatorial storm could have had a similar perturbing effect on the QPO (magnified as it occurred at a location geographically closer to the meteorological activity responsible for the QPO), this still cannot explain the mismatch of phase between the Voyager and Cassini observations[22] as the oscillation appeared well behaved in the ground-based time series during this period[3]. Conversely, the phase of the QPO may influence Saturn's extra-tropical circulation via secondary circulations, modulating temperatures at mid-latitudes and changing the atmospheric susceptibility to large-scale convective eruptions like that seen in 2010. The key conclusion of this work is that a gas giant's equatorial oscillation can respond to meteorology elsewhere on the planet, just like Earth's QBO. The same could be true of Jupiter's QQO, provided that waves spawned by jovian convective storms are able to interact with the QQO shear zones (that is, that they can overcome confinement barriers in latitude and altitude). Stratospheric waves over Jupiter's equatorial belts have been observed in relation to tropospheric plume events[29], but a comprehensive survey relating QQO changes to Jupiter's belt and zone upheavals is not yet available. Nevertheless, this disruption to Saturn's QPO supports the view of giant-planet atmospheres as intricately interconnected systems.

Methods

Cassini/CIRS spectra. This study employs Cassini/CIRS[23] interferograms of Saturn taken between March 2004 and November 2016. We use 15-cm^{-1} spectral resolution mid-infrared observations spanning 600–1,400 cm^{-1} (7.1–16.6 μm) acquired using CIRS focal planes 3 and 4, where each pixel covers a 0.273-mrad^2 instantaneous field of view. In addition, we truncated longer CIRS interferograms that had been designed to produce higher spectral resolutions (2.5 cm^{-1}) to expand the 15-cm^{-1} dataset. Interferograms were calibrated and converted to spectra that were co-added on a 1-month time grid and a 2°-wide latitudinal grid (with 1° step size). Both prime CIRS-targeted observations, and observations 'riding along' with other Cassini instruments, are employed to expand the time series, following techniques described in ref. [30]. This results in the temporal coverage of Saturn's low latitudes as shown in Supplementary Fig. 1. Note that the spectra are not truly zonally averaged, as CIRS did not acquire full 360° longitude coverage every month. However, away from Saturn's storm, the planet's temperature structure is nearly axially symmetric, such that the co-added spectra represent good approximations to the zonal mean (note that this is not true of latitudes 30–60° N during the 2011–2014 epoch, which is why these latitudes are omitted from the main text). Furthermore, we assessed all CIRS maps that did cover 360° of longitude during the storm epoch (2011–2013). Although horizontal wave activity was present, we did not detect significant longitudinally localized perturbations in the temperatures at low latitudes. We conclude that the wave-induced momentum changes acted at all longitudes.

Spectral inversion and information content. Cassini CIRS spectra of Saturn are characterized by a host of stratospheric emission features (for example, ethane, acetylene and methane) and tropospheric absorption features (for example, phosphine) superimposed onto the broad collision-induced absorption spectrum of H_2–H_2 and H_2–He. These are inverted using an optimal estimation retrieval algorithm, NEMESIS[31], based on the formalism of optimal estimation developed by the Earth-observing community[32]. Inversions balance the goodness-of-fit to the spectral data against constraints imposed by a priori information—specifically, the vertical temperature and gaseous profiles provided by previous studies (see ref. [13] for full details of the inversion procedure, sources of spectral line data and previous distributions, and the conversion of line data to *k*-distributions for rapid calculation of atmospheric transmission). Uncertainties on the retrieved temperatures depend on measurement errors, uncertainties in spectral line data, assumptions about vertical smoothing in the retrieval process, and correlations between parameters. Temperature uncertainties range from ~3 K at the tropopause, to 1.5–2.0 K near 200 mbar (the peak of the tropospheric contribution), 3.5–4.5 K at 1–5 mbar (the peak of the stratospheric contribution). The same time-independent and latitude-independent a priori initial profile was used for all inversions, based on a combination of low-latitude nadir and limb inversions from previous studies[9,20], so as not to introduce biases in the results. Retrieved

temperatures representative of the zonal mean at 0.5, 1.0 and 5.0 mbar are shown in Supplementary Fig. 2. The temperatures at individual latitudes and pressures were then interpolated (Supplementary Fig. 3) to produce Fig. 1. The temporal evolution of these interpolated temperatures, and their associated temperature anomalies, is shown in Supplementary Fig. 4 for a range of latitudes.

This study utilizes nadir data only (defined in this context as any observation with an emission angle less than 60°), and so vertical information content is low, particularly in the middle atmosphere. Temperature gradients can only be reliably extracted in the 0.5–5.0 mbar range, and even then, they would underestimate any sharp vertical gradients in temperature. The nadir 600–1,400 cm^{-1} data have no sensitivity to temperatures in the 5–80 mbar range, meaning that latitudinal thermal gradients ($\partial T/\partial y$) will not be accurately determined from nadir data alone. Supplementary Figs. 5 and 6 compare nadir spectral inversions at 0.5, 2.5 and 15.0 cm^{-1} to CIRS limb observations previously published[3,9]. Higher spectral resolutions better resolve the shapes of the spectral lines to extract more vertical information. Allowing for differences in the observing strategies, the comparison between the two independent retrieval methods is favourable in the 0.5–5.0 mbar range. Some discrepancies do exist that are outside of our formal retrieval uncertainties in the 0.5–5.0 mbar range, but these are likely to be due to incomplete spatial sampling on Saturn, particularly during the storm epoch.

Offsets between the two data types (nadir and limb) are larger at 10 mbar, where only the limb data offer any constraint. Nadir sensitivity is dramatically reduced at these pressures as the Planck function of the CH_4 emission drops sharply due to the cooler temperatures for $p > 5$ mbar. This poses a significant problem for stratospheric wind-speed estimates via the thermal wind equation, as we describe below. As a cross-check that the QPO perturbation is a real phenomenon in Saturn's atmosphere, Supplementary Fig. 7 presents the same time series as Supplementary Fig. 3, but using only 2.5-cm^{-1} observations at their native spectral resolution. These have poorer temporal sampling, but show the same trends as the 15-cm^{-1} dataset.

Thermal winds. Estimation of stratospheric zonal winds (u) rely on integrations of the cloud-tracked zonal winds using the measured temperature gradients, $\partial T/\partial y$. The standard thermal wind equation (TWE) relates zonal vertical windshears to meridional temperature gradients in pressure $\left(\frac{\partial u}{\partial z} = -\frac{g}{fT}\frac{\partial T}{\partial y}\right)$

where z is the altitude, f is the Coriolis parameter ($f = 2\Omega\sin\varphi$ where φ is the planetographic latitude and Ω is the planetary rotation rate), and g is the local acceleration of gravity. This equation breaks down at low latitudes as the Coriolis parameter tends towards zero. Geostrophic balance can still apply at the equator, but computation of zonal winds is impracticable due to error amplification in altitude owing to the small value of f. Away from the equator, and for thin atmospheres, the wind gradient is vertical. However, it was shown in ref. [33] that the integration of the TWE near the equator must be along cylinders concentric with the rotation axis ($z_{||}$,rather than with altitude, as in the standard TWE). We estimated the zonal winds using this modified TWE using two different approaches[9,19] and found both to be consistent with one another. Following ref. [9], the modified TWE can be expressed as:

$$\frac{\partial}{\partial z_{||}}\left(2\Omega u + \frac{u^2}{r\cos\varphi_c}\right) = -\frac{g}{T}\frac{1}{r}\left(\frac{\partial T}{\partial \varphi_p}\right)_p$$

where r is the local radius, and φ_c and φ_p are planetocentric and planetographic latitudes, respectively. We display temporal trends in the thermal windshear along these cylinders in Fig. 3c and Supplementary Fig. 8. Furthermore, Supplementary Fig. 9 demonstrates that the vertical windshear (from the standard TWE, omitting low latitudes where errors are magnified) and the windshear along cylinders (from the modified TWE) are morphologically similar, but the latter is the correct form to use at the equator.

Integration of the modified TWE requires a selection of boundary conditions. We can choose to (i) use the cloud-top winds from continuum-band imaging[25] as our boundary condition at 500 mbar, following previous wind calculations[19,26]; or (ii) specify an artificial level of zero motion ($u = 0$ m s^{-1}) at an altitude just below our region of vertical sensitivity, following ref. [4]. Note that we do not expect a zero-wind level in the 5–70 mbar range, as Cassini cloud tracking in methane-band imaging[34] suggests that the winds are still strong and eastward at the 50-mbar level. The winds presented in the $p < 5$ mbar range in Figs. 2 and 3 should therefore be considered as a 'delta' on top of the background flow. Furthermore, the modified TWE can only be integrated for latitudes where the tangent cylinders intersect the reference pressure p_0 where the boundary condition is specified. If the tangent cylinder intersects lower pressures, then no boundary condition is available for the wind integration (that is, we do not know the zonal velocity in the equatorial plane for $p < p_0$ mbar). This 'no-solution' region is defined by a parabola, centred on the equator, in Fig. 2 and the Supplementary Information. In producing the temporal plots in Fig. 3, we extrapolated through the 'no-solution' region to the equator so that the values represent those calculated at the edge of the no-solution parabola.

Supplementary Fig. 10 contrasts the wind calculations for zero-motion levels at 5, 10 and 20 mbar, with a full calculation assuming the Cassini cloud-tracked winds at 500 mbar. Although the latter matches calculations from refs [19,34], the wind speeds are deemed to be unrealistically large for two reasons: (i) the nadir data do not adequately constrain meridional temperature gradients in the 5–80 mbar range; and (ii) the vertical resolution of nadir inversions is sufficiently poor that regions of windshear are smeared out over broad altitude ranges. As limb inversions have shown that $\partial T/\partial y$ at 10 mbar is generally opposite to that at 1 mbar (Supplementary Fig. 5), a nadir-only wind calculation will be severely biased to the $\partial T/\partial y$ measured in the 1-mbar region, leading to a substantial overestimation of winds there. This explains why the magnitude of the 1-mbar jet from nadir inversions[19,26] is significantly larger than that from limb inversions[4,9]. CIRS limb analyses suggest an ~300 m s^{-1} difference between zonal winds in the eastward and westward shear zones[9]. Figure 3d uses a zero-motion constraint at 5 mbar and finds an ~600 m s^{-1} difference from 2005 to 2016, so we estimate that nadir-derived zonal-wind contrasts are subject to uncertainty factors of approximately 2–3. However, placement of the zero-motion boundary at higher pressures (Supplementary Fig. 10) makes this contrast even larger, highlighting the uncertainty in absolute wind measurements.

The estimated windshear and zonal winds are compared in Supplementary Fig. 8 for both scenarios (that is, integrating only for $p < 5$ mbar, and integrating for $p < 500$ mbar). The latter suggests that stratospheric winds turn retrograde in the westward QPO phase, but we consider this unlikely given the strong prograde flow at Saturn's equator at the cloud tops, and is an artefact of our lack of knowledge of the $\partial T/\partial y$ structure in the lower stratosphere. Although Cassini limb observations could help to resolve this conundrum, they are too infrequent to develop a proper time series of the varying 10–50 mbar temperature gradients, so only nadir data can reveal the middle-atmosphere changes associated with this storm over short timescales. This remains a fundamental limitation of determining winds from nadir spectroscopy at low spectral resolutions.

Ground-based thermal observations. In addition to Cassini observations of the vertical structure of the equatorial oscillation, Saturn's QPO was also discovered in the thermal contrasts displayed in ground-based imaging sensitive to stratospheric methane (7.9 μm) and ethane (12.3 μm)[3]. This imaging programme, using the Subaru Telescope and Very Large Telescope, has continued throughout the Cassini mission, and proved instrumental in tracking the evolution of the 2010 storm and its stratospheric vortex[13]. Using the CIRS time series generated from the spline interpolation of the inversions[38], we forward-modelled the expected radiances in typical 7.9- and 12.3-μm filters, taking care to use the correct observational geometry for Earth-based facilities. The effects of the 2011–2013 equatorial cooling can clearly be seen in both filters in Supplementary Fig. 11, and these data confirm the change in the QPO phase. Furthermore, if we compute the same contrast-index as in ref. [3]—namely, the difference between 3.5° N and 15.5° N (red lines in Supplementary Fig. 11) and 3.5° S and 15.5° S (blue lines in Supplementary Fig. 11, all latitudes planetographic)—we can compare the simulation to observations. We consider data from (1) the VLT VISIR instrument[35], from 2008 (program ID: 381. C-0560), 2009 (383.C-0164), 2010 (084.C-0193) and 2011 (287.C-5032), and then more recently in 2015 (095.C-0142) and 2016 (097.C-0226); and (2) the Subaru COMICS instrument[36,37] from 2005 to 2009 in programs S05A-029, S07B-015, S07B-076 and S08B-023. Subsets of the VISIR 7.9-μm observations are shown in Fig. 1 and Supplementary Fig. 12. Data were reduced, remapped and calibrated using techniques described in ref. [39]. The equatorial region (±3.5°) was warmer than the tropical latitudes (±15.5°) at 7.9 μm until 2010–2011. After this time, the whole ±20° latitude range grew cooler, and the contrast between the equator and tropical latitudes reversed. By the end of the sequence, the warm equatorial band described in ref. [3] had been replaced by a cool equatorial band. Unfortunately, the data in Supplementary Fig. 11 lack the time coverage to add more detail to the rapid changes in 2011. Furthermore, images in 2011 were dominated by the intense brightness of the stratospheric vortex, making it difficult to observe the equatorial contrasts from Earth. This Earth-based programme will continue beyond the end of Cassini's mission in 2017 to track the expected return of the warm equatorial band in 7.9-μm imaging, which can be seen forming at low pressure ($p < 0.5$ mbar) at the end of the Cassini time series.

Data availability. This work relies on two data sources—Cassini and ground-based data. Calibrated Cassini/CIRS spectra and raw interferograms are available via the Planetary Data System (http://atmos.nmsu.edu/pdsd/archive/data/co-s-cirs-234-tsdr-v32/). Co-added spectra, retrieved atmospheric temperatures, spline-interpolated temperatures and other derived products are available from the corresponding author. Raw VLT/VISIR images from 2008–2016 are available via the archive of the European Southern Observatory (http://archive.eso.org). Raw Subaru/COMICS images from 2005–2009 are available via the SMOKA Science Archive (http://smoka.nao.ac.jp/). Calibrated images and maps are available from the corresponding author.

Received: 13 June 2017; Accepted: 5 September 2017;
Published online: 23 October 2017

References

1. Baldwin, M. P. et al. The quasi-biennial oscillation. *Rev. Geophys.* **39**, 179–229 (2001).
2. Leovy, C. B., Friedson, A. J. & Orton, G. S. The quasiquadrennial oscillation of Jupiter's equatorial stratosphere. *Nature* **354**, 380–382 (1991).
3. Orton, G. et al. Semi-annual oscillations in Saturn's low-latitude stratospheric temperatures. *Nature* **453**, 196–198 (2008).
4. Fouchet, T. et al. An equatorial oscillation in Saturn's middle atmosphere. *Nature* **453**, 200–202 (2008).
5. Reed, R. J., Campbell, W. J., Rasmussen, L. A. & Rogers, D. G. Evidence of downward propagating annual wind reversal in the equatorial stratosphere. *J. Geophys. Res.* **66**, 813–818 (1961).
6. Ebdon, R. A. Notes on the wind flow at 50 mb in tropical and sub-tropical regions in January 1957 and January 1958. *Q. J. R. Meteorol. Soc.* **86**, 540–542 (1960).
7. Osprey, S. M. et al. An unexpected disruption of the atmospheric quasi-biennial oscillation. *Science* **353**, 1424–1427 (2016).
8. Newman, P. A., Coy, L., Pawson, S. & Lait, L. R. The anomalous change in the QBO in 2015-2016. *Geophys. Res. Lett.* **43**, 8791–8797 (2016).
9. Guerlet, S., Fouchet, T., Bézard, B., Flasar, F. M. & Simon-Miller, A. A. Evolution of the equatorial oscillation in Saturn's stratosphere between 2005 and 2010 from Cassini/CIRS limb data analysis. *Geophys. Res. Lett.* **38**, L09201 (2011).
10. Fletcher, L. N. et al. Thermal structure and dynamics of Saturn's northern springtime disturbance. *Science* **332**, 1413–1417 (2011).
11. Sanchez-Lavega, A. et al. Deep winds beneath Saturn's upper clouds from a seasonal long-lived planetary-scale storm. *Nature* **475**, 71–74 (2011).
12. Fischer, G. et al. A giant thunderstorm on Saturn. *Nature* **475**, 75–77 (2011).
13. Fletcher, L. N. et al. The origin and evolution of Saturn's 2011–2012 stratospheric vortex. *Icarus* **221**, 560–586 (2012).
14. Friedson, A. J. New observations and modelling of a QBO-like oscillation in Jupiter's stratosphere. *Icarus* **137**, 34–55 (1999).
15. Lindzen, R. S. & Holton, J. R. A theory of the quasi-biennial oscillation. *J. Atmos. Sci.* **25**, 1095–1107 (1968).
16. Holton, J. R. & Lindzen, R. S. An updated theory for the quasi-biennial cycle of the tropical stratosphere. *J. Atmos. Sci.* **29**, 1076–1080 (1972).
17. Andrews, D. G., Holton, J. R. & Leovy, C. B. *Middle Atmosphere Dynamics* (Academic Press, New York, 1987).
18. Schinder, P. J. et al. Saturn's equatorial oscillation: evidence of descending thermal structure from Cassini radio occultations. *Geophys. Res. Lett.* **38**, L08205 (2011).
19. Li, L. et al. Strong jet and a new thermal wave in Saturn's equatorial stratosphere. *Geophys. Res. Lett.* **35**, L23208 (2008).
20. Fletcher, L. N. et al. Seasonal change on Saturn from Cassini/CIRS observations, 2004–2009. *Icarus* **208**, 337–352 (2010).
21. Li, L. et al. Strong temporal variation over one Saturnian year: from Voyager to Cassini. *Sci. Rep.* **3**, 2410 (2013).
22. Sinclair, J. A. et al. From Voyager-IRIS to Cassini-CIRS: interannual variability in Saturn's stratosphere? *Icarus* **233**, 281–292 (2014).
23. Flasar, F. M. et al. Exploring the Saturn system in the thermal infrared: the composite infrared spectrometer. *Space Sci. Rev.* **115**, 169–297 (2004).
24. Garcıa-Melendo, E. & Sanchez-Lavega, A. Shallow water simulations of Saturn's giant storms at different latitudes. *Icarus* **286**, 241–260 (2017).
25. Garcıa-Melendo, E., Perez-Hoyos, S., Sanchez-Lavega, A. & Hueso, R. Saturn's zonal wind profile in 2004-2009 from Cassini ISS images and its long-term variability. *Icarus* **215**, 62–74 (2011).
26. Read, P. L. et al. Mapping potential vorticity dynamics on Saturn: zonal mean circulation from Cassini and Voyager data. *Planet. Space Sci.* **57**, 1682–1698 (2009).
27. Achterberg, R. K. & Flasar, F. M. Planetary-scale thermal waves in Saturn's upper troposphere. *Icarus* **119**, 350–369 (1996).
28. Scaife, A. A. et al. Predictability of the quasi-biennial oscillation and its northern winter teleconnection on seasonal to decadal timescales. *Geophys. Res. Lett.* **41**, 1752–1758 (2014).
29. Fletcher, L. N. et al. Moist convection and the 2010-2011 revival of Jupiter's South Equatorial Belt. *Icarus* **286**, 94–117 (2017).
30. Fletcher, L. N. et al. Seasonal evolution of Saturn's polar temperatures and composition. *Icarus* **250**, 131–153 (2015).
31. Irwin, P. et al. The NEMESIS planetary atmosphere radiative transfer and retrieval tool. *J. Quant. Spectrosc. Radiat. Transf.* **109**, 1136–1150 (2008).
32. Rodgers, C. D. *Inverse Methods for Atmospheric Remote Sounding: Theory and Practice* (World Scientific, Singapore, 2000).
33. Flasar, F. M. et al. Titan's atmospheric temperatures, winds, and composition. *Science* **308**, 975–978 (2005).
34. Li, L. et al. Equatorial winds on Saturn and the stratospheric oscillation. *Nat. Geosci.* **4**, 750–752 (2011).
35. Lagage, P. O. et al. Successful commissioning of VISIR: the mid-infrared VLT instrument. *The Messenger* **117**, 12–16 (2004).
36. Kataza, H. et al. COMICS: the cooled mid-infrared camera and spectrometer for the Subaru telescope. *Proc. SPIE* **4008**, 1144–1152 (2000).
37. Okamoto, Y. K. et al. Improved performances and capabilities of the cooled mid-infrared camera and spectrometer (COMICS) for the Subaru telescope. *Proc. SPIE* **4841**, 169–180 (2003).
38. Teanby, N. Constrained smoothing of noisy data using splines in tension. *Math. Geol.* **39**, 419–434 (2007).
39. Fletcher, L. N. et al. Retrievals of atmospheric variables on the gas giants from ground-based mid-infrared imaging. *Icarus* **200**, 154–175 (2009).

Acknowledgements

L.N.F. was supported by a Royal Society Research Fellowship and European Research Council Consolidator Grant (under the European Union's Horizon 2020 research and innovation programme, grant agreement no. 723890) at the University of Leicester. The UK authors acknowledge the support of the Science and Technology Facilities Council. S.G. and T.F. were supported by the Centre national d'études spatiales. A portion of this work was completed by G.S.O. at the Jet Propulsion Laboratory, California Institute of Technology, under contract with NASA. We are extremely grateful to all those Cassini team members involved in the planning, execution and reduction of the CIRS data, without whom this study would not have been possible. This investigation was partially based on VLT observations collected at the European Organisation for Astronomical Research in the Southern Hemisphere (see Extended Data for ESO program IDs); and on data acquired by the Subaru Telescope operated by the National Astronomical Observatory of Japan, and extracted from the SMOKA database (program IDs are provided in the Extended Data).

Author contributions

L.N.F. was responsible for analysing the nadir data and writing the article. S.G. and T.F. analysed Cassini limb observations and assisted with the nadir–limb comparison and calculation of zonal winds. L.L. provided a cross-comparison of zonal winds via a different algorithm, and F.M.F. provided assistance with the wind calculations. G.S.O. assisted with the ground-based observing campaign. P.G.J.I. developed the software to permit inversions of Cassini/CIRS spectra. N.G. generated the CIRS spectral database. All authors read and commented on the manuscript.

Competing interests

The authors declare no competing financial interests.

Additional information

Supplementary information is available for this paper at https://doi.org/10.1038/s41550-017-0271-5.

Reprints and permissions information is available at www.nature.com/reprints.

Correspondence and requests for materials should be addressed to L.N.F.

Publisher's note: Springer Nature remains neutral with regard to jurisdictional claims in published maps and institutional affiliations.